Effects of Surface Geometry on the Wenzel-to-Cassie Transition of a Water Droplet

Hyojeong Kim,[†] Man Yeong Ha,[‡] and Joonkyung Jang[†,*]

[†]*Department of Nanoenergy Engineering, Pusan National University, Busan 46241, Republic of Korea.*
**E-mail: jkjang@pusan.ac.kr*
[‡]*School of Mechanical Engineering, Pusan National University, Busan 46241, Republic of Korea*
Received May 31, 2017, Accepted June 24, 2017, Published online July 26, 2017

The Wenzel (WZ) to Cassie-Baxter (CB) transition of a water droplet on a periodic array of pillars was investigated theoretically. Treating the WZ to CB transition as a phase transition, an analytical theory was developed previously for the threshold value of the inter-pillar spacing, S_T, below which the WZ to CB transition occurs. Herein, the theory of S_T was applied to the square array of rectangular, cylindrical, or ellipsoidal pillars with a range of experimental sizes. The behavior of S_T was examined by varying the height and width of the pillars. The theory is shown to agree well with previous experiments. The present analytic expressions of S_T can provide guidelines for designing the surface structure forming the CB states of water droplets.

Keywords: Wenzel, Cassie-Baxter, Phase transition, Superhydrophobic surface, Wetting, Drying

Introduction

Super-hydrophobic surfaces have extensive applications, such as water harvesting,[1] impermeable textiles,[2,3] anti-fogging,[4] self-cleaning paints, and glass windows.[5,6] Typically, a water droplet on a super-hydrophobic surface has a static contact angle greater than 150° and a sliding angle less than 5°.[7] Such ultra-hydrophobicity can be achieved by decorating the surface with an array of microscale pillars. Lotus leaves, which have extremely high water repellency,[8–11] have numerous micro pillars on their surfaces.[12–14] With the advances in nano- and micro-electromechanical systems (NEMS and MEMS) technologies, various shapes of pillars can be constructed on the micro- or nano-scale. The most widely manufactured arrays are arrays of rectangular, cylindrical, or ellipsoidal pillars, even though more sophisticated structures, such as mushroom-like and dual-scale pillars are possible in principle.[15,16]

A water droplet resting on a pillared surface takes a Wenzel (WZ) or Cassie-Baxter (CB) state. In the WZ state, a water droplet fills the gap (groove) between pillars, fully contacting the side walls of pillars (see Figure 1).[17] In the CB state, however, the droplet only contacts the tops of the pillars while the sidewalls of the pillars are dry. In other words, the inter-pillar gap is filled with a liquid in the WZ state,[18] whereas the gap is in a vapor phase in the CB state.[19] A water droplet in the CB state has an enhanced contact angle and mobility[20]; therefore, a pillared surface with a CB state is desired.

The WZ or CB state of a water droplet on a pillared surface is determined by the surface geometry: shape, height H, and width W of each pillar; and the spacing between neighboring pillars, S (Figure 2). Knowing whether a droplet is in the WZ or CB state is essential for predicting the contact angle of that droplet using the CB,[19] WZ,[18] or more advanced theory.[21–24] A water droplet has a maximal contact angle, hence maximal hydrophobicity,[25] at the geometry near the CB to WZ transition. Therefore, understanding how these geometrical parameters affect the WZ or CB state of a droplet provides important guidelines for designing super-hydrophobic surfaces. Unfortunately, controlling and scanning of these geometric parameters to determine the optimal surface geometry (combination of H, W, and S) experimentally are challenging, time consuming, and expensive. In this respect, a simple theory capable of predicting the WZ or CB state of a droplet on a pillared surface is desired.

The CB or WZ state of a water droplet is determined by competition between the intermolecular cohesion and interfacial energy of water confined between the pillars; as S decreases, the water confined between the pillars decreases its volume and hence its degree of cohesion. Below a certain threshold value, S_T, the confined water is destabilized and evaporates because of the dominance of the liquid–solid interfacial energy, giving rise to a CB state.[26–32] Therefore, the WZ to CB (CB to WZ) transition can be viewed as a drying (condensation) transition. Based on this view, a simple analytical theory for S_T was developed. The closed-form expression of S_T was obtained for a square array of rectangular, cylindrical, or ellipsoidal pillars as a function of W and H of a pillar for a given pressure of a water droplet, P.

The theory was compared with Monte Carlo[33–35] and molecular dynamics[36,37] simulations and shown to agree. Owing to the limited sizes of the molecular simulations, however, the previous applications of the theory were limited to nanoscale pillars. On the other hand, typical pillars in experiments are on the micrometer scale. Herein, the

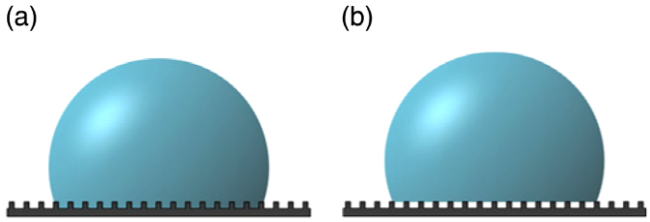

Figure 1. Schematic diagrams of the Wenzel (a) and Cassie-Baxter (b) states of a water droplet on a periodic array of pillars.

theory of S_T was applied to pillars with various experimental sizes and shapes. This study investigated how S_T behaves by systematically varying the geometric parameters of pillars: W, H, and S. The theory was tested and showed good agreement with previous experiments.

Theory

The following summarizes the theory detailed in previous work.[34] In both WZ and CB states, it is assumed that a macroscopic water droplet is sitting on top of pillars (Figure 2(a)–(c), $z > H$), and the inter-pillar gap is negligibly small compared to the droplet. The difference between the grand potentials of the liquid and vapor confined in the gap between pillars ($z < H$), $\Delta\Omega$, is given by

$$\Delta\Omega = \mathrm{PV} + \gamma_{LV}\cos\theta_f A_S + \gamma_{LV}A_{LV}, \quad (1)$$

where V is the volume of the gap between the side walls of the neighboring pillars; A_S and A_{LV} are the areas of the side walls of the pillars and the liquid–vapor interface in the CB state, respectively. P is the pressure of the liquid droplet in excess of the vapor pressure. γ_{LV} is the liquid–vapor interfacial tension, and θ_f is the intrinsic contact angle of the droplet on a *flat* surface (see figure 2(d)).

By imposing $\Delta\Omega = 0$ at $S = S_T$, S_T can be derived for an infinite square array of rectangular pillars as follows:

$$S_T = W\left[\sqrt{1-\frac{4r\gamma_{LV}\cos\theta_f}{\{\mathrm{Pr}W+\gamma_{LV}(\cos\theta_f+1)\}}}-1\right], \quad (2)$$

where r is the aspect ratio, $r = H/W$. The S_T for an array of cylindrical pillars is given by

$$S_T = W\left[\left(\frac{\sqrt{\pi}}{2}\right)\sqrt{1-\frac{4r\gamma_{LV}\cos\theta_f}{\{\mathrm{Pr}W+\gamma_{LV}(\cos\theta_f+1)\}}}-1\right]. \quad (3)$$

Similarly, S_T for an array of ellipsoidal pillars is given by

$$S_T = W\left[\left(\sqrt{\frac{\pi}{6}}\right)\sqrt{\frac{\mathrm{Pr}W}{\{\mathrm{Pr}W+\gamma_{LV}(\cos\theta_f+1)\}}-\frac{3r\gamma_{LV}\cos\theta_f\{\arcsin(K)/K\}}{\{\mathrm{Pr}W+\gamma_{LV}(\cos\theta_f+1)\}}}-1\right], \quad (4)$$

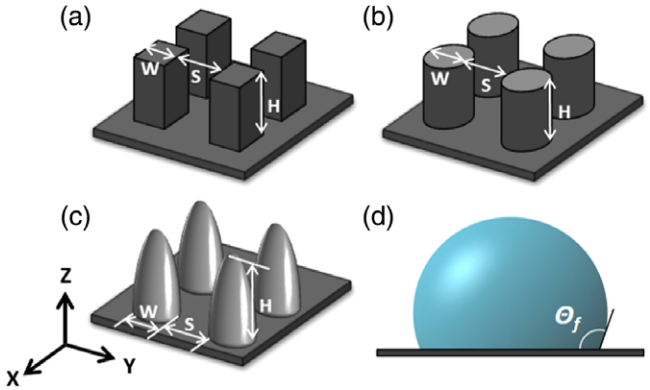

Figure 2. Periodic square arrays of pillars studied (a)–(c) and schematic diagram of the intrinsic contact angle θ_f of the droplet on a flat surface (d). Arrays of rectangular (a), cylindrical (b), and ellipsoidal (c) pillars are considered. W, H, and S are the width and height of each pillar and the inter-pillar spacing between the neighboring pillars, respectively.

where $K = \sqrt{1-1/(4r^2)}$.

Consider the limiting cases by fixing the aspect ratio in Eqs (2)–(4). In the limit of a vanishingly small pillar width, $W \to 0$, Eqs (2)–(4) all reduce to $S_T \to 0$. Note the height of a pillar also vanishes in this limit (because of the fixed aspect ratio). As the liquid on top of the pillars easily fills the gap between extremely short pillars, the only way to dry out the inter-pillar gap is to reduce S to zero. In a large W limit, Eq (2) approaches a constant independent of the aspect ratio:

$$S_T \to -\frac{2\gamma_{LV}\cos\theta_f}{P}. \quad (5)$$

In contrast, the S_T for cylindrical and ellipsoidal pillars becomes a linearly decreasing function of W,

$$S_T \to -\frac{\sqrt{\pi}(\gamma_{LV}\cos\theta_f)}{P}-\left(1-\frac{\sqrt{\pi}}{2}\right)W, \quad (6)$$

$$S_T \rightarrow -\frac{\gamma_{LV}}{2r}\left(\sqrt{\frac{\pi}{6}}\right)\left[\frac{(\cos\theta_f+1)}{P} + \frac{3r\cos\theta_f\{\arcsin(K)/K\}}{P}\right] - \left(1-\sqrt{\frac{\pi}{6}}\right)W. \quad (7)$$

Note that the limiting value of S_T for an array of cylindrical pillars is independent of r, whereas the limit for an array of ellipsoidal pillars depends on r.

S_T given by Eqs (6) or (7) reaches zero at a sufficiently large W. In other words, a water droplet on cylindrical or ellipsoidal pillars cannot take the CB state above a threshold value, W_T. From Eqs (3) and (4), the W_Ts for cylindrical and ellipsoidal pillars, respectively, are given by

$$W_T = \left\{\frac{\gamma_{LV}\cos\theta_f}{(1/4-1/\pi)} - \frac{\gamma_{LV}(\cos\theta_f+1)}{r}\right\}\left(\frac{1}{P}\right), \quad (8)$$

and

$$W_T = \frac{\gamma_{LV}[2(\cos\theta_f+1)+\pi r\cos\theta_f\{\arcsin(K)/K\}]}{r(\pi/3-2)}\left(\frac{1}{P}\right). \quad (9)$$

Eqs (8) and (9) were newly developed in this study. The absence of a CB state for large values of W can be understood as follows. Unlike the case of rectangular pillars, the inter-pillar gap does not vanish by making $S = 0$ for cylindrical or ellipsoidal pillars. With increasing W, the liquid confined between the cylindrical or ellipsoidal pillars at $S = 0$ should increase in both volume and contact area with pillar walls. It turns out that the increase in the volume is faster than the increase in surface area.[33] Consequently, the cohesion of liquid (which scales with volume) dominates over the hydrophobic surface (liquid–pillar interface) effect. The WZ state is then always more stable than the CB state above a threshold value, W_T, as given by Eqs (8) and (9). These results have important implications for designing pillared surfaces. A hydrophobic surface texturized with rectangular pillars is guaranteed to generate the CB state of a droplet. In contrast, a surface decorated with cylindrical or ellipsoidal pillars cannot induce a CB state if the pillars are too wide (note also the aspect ratio is fixed here).

This study investigated how S_T depends on the pillar width, W, by fixing the aspect ratio ($r = H/W$) to 2, a typical value for pillared surfaces in experiments. Figure 3 presents plots of S_T vs. W for arrays of rectangular (solid lines), cylindrical (broken lines), and ellipsoidal (dotted lines) pillars. The results are shown for a high (1 MPa, top) and a low (144 Pa, bottom) pressure of the droplet, P. The intrinsic contact angle was taken from the experimental value for a *flat* silicon surface coated with a plasma-polymerized fluorocarbon (111.5°).[25] Throughout this work, an experimental surface tension value of γ_{LV} (= 72.1 mN/m) was used. As shown in the figure, the S_T values for the arrays of rectangular pillars are larger than those for the arrays of the cylindrical and ellipsoidal pillars. This is because at the same value of S, the liquid confined between the rectangular pillar walls has a smaller volume than that of the cylindrical or ellipsoidal pillars. To have the same volume between the pillar walls, the inter-pillar spacing for the rectangular pillars should be larger than that for cylindrical or ellipsoidal pillars. Consequently, the WZ to CB transition occurs at a larger S value for an array of rectangular pillars.

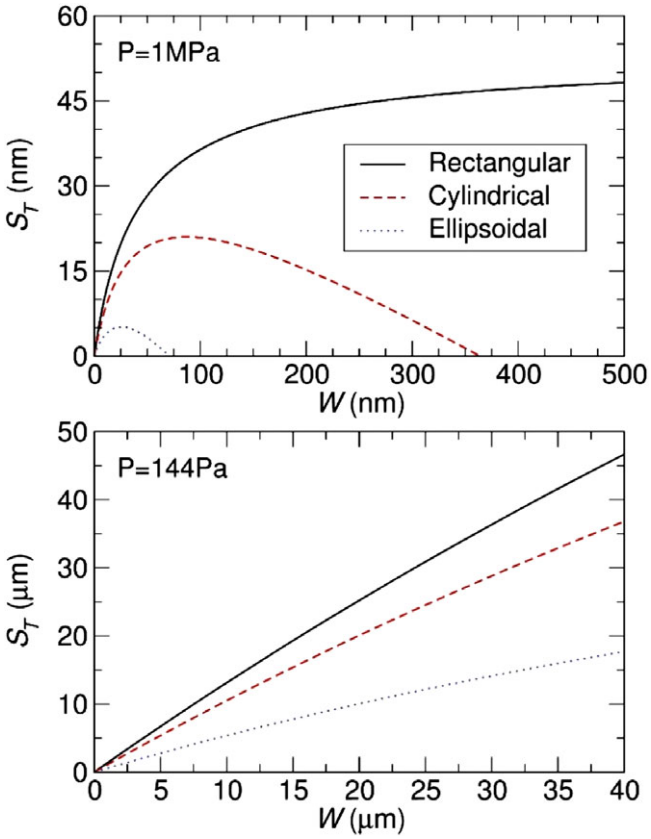

Figure 3. Threshold inter-pillar spacing S_T vs. the width of pillar for a fixed aspect ratio. Two different Ps of 1 MPa (top) and 144 Pa (bottom) are considered. The theoretical S_T is drawn for the square arrays of rectangular, cylindrical, and ellipsoidal pillars as the solid, broken, and dotted lines, respectively.

Consider the case, $P = 1$ MPa which is relevant to the pressure of a droplet colliding with a surface with a speed of 6 m/s.[38] With increasing W, S_T for an array of rectangular pillars increases gradually and reaches a plateau (S_T = 50.4 nm). For the arrays of cylindrical and ellipsoidal pillars however, S_T first increases and then decreases with increasing W. S_T for cylindrical pillars reaches a maximum of $S_T = 21$ nm at $W = 87.2$ nm, then decreases and becomes zero at $W = 364$ nm. For an array of ellipsoidal pillars, S_T reaches a maximum at $W = 25.5$ nm with increasing W, then decreases to zero at $W = 70.6$ nm. Consequently, above a threshold value of W, W_T, the droplet on

an array of cylindrical or ellipsoidal pillars always remains in the WZ state. As discussed above, the inter-pillar gap does not vanish by making $S = 0$, for an array of cylindrical or ellipsoidal pillars. As the width of the pillar increases at $S = 0$ with an aspect ratio fixed to 2, the increase in volume between the pillar walls is faster than that in the surface area. Consequently, the cohesion of liquid scaling with volume dominates the hydrophobic surface effect for W. Therefore, the WZ state is always more stable than CB for $W > W_T$.

Consider the lower pressure case, $P = 144$ Pa, which is relevant to the pressure of a static droplet with a radius of 1 mm (according to the Young-Laplace equation, $P = 2\gamma_{LV}/R$). The S_T vs. W curve shows that the CB state exists regardless of the pillar shape in the typical range of experimental widths, $W \leq 50$ μm, generated in MEMS or NEMS. As observed for the high-pressure case (top of Figure 3), S_T for a given W increases as the pillar shape changes from ellipsoidal to cylindrical and to rectangular. The threshold, W_T, can be estimated as 2.53 mm and 491 μm for cylindrical and ellipsoidal pillars, respectively.

Comparison with Experiments and Discussion

This theory was assessed by a comparison with the experimental data provided by Zhu *et al.*[39] who measured S_T for the CB to WZ transition by carefully controlling and scanning the surface geometry. Figure 4 shows the results for five different combinations of the width and aspect ratios of rectangular pillars. In this calculation, the pressure of the droplet, P, was obtained using the Young-Laplace equation, where the radius of droplet R was taken to be 1 mm. The intrinsic contact angle, 111.8°, reported in their experiment was used.[39] Figure 4 presents the theoretical S_T vs. W curves for five different aspect ratios as lines. The theoretical S_T agrees well with the experimental results; the experimental S_T values (filled symbols, group 1 of Table 2 in Zhu *et al.*[39]) almost fall on the theoretical curves. The relative deviation of the experiment from theory ranged from 0.3 to 5.9%.

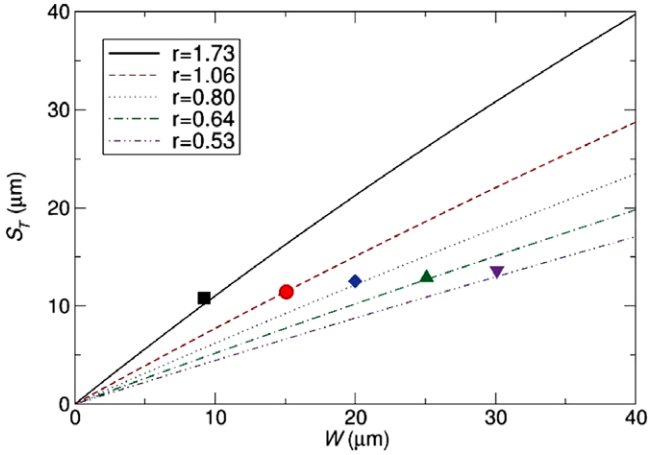

Figure 4. Comparison of the theoretical S_T with that of the experiment by Zhu *et al.*[39] The theoretical S_T for an array of rectangular pillars is plotted vs. W for five different aspect ratios, rs, used in the experiment (0.53, 0.64, 0.80, 1.06, and 1.73). The theoretical and experimental S_T values are drawn as lines and filled symbols, respectively.

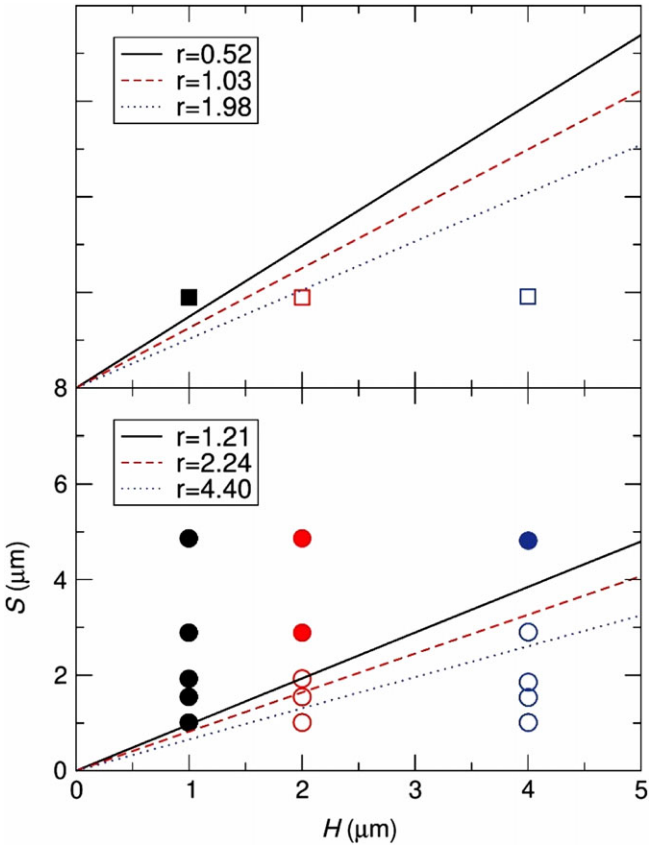

Figure 5. Theoretical prediction of the CB or WZ state for different combinations of H and S. The theoretical S_T vs. H is drawn as a line for the arrays of rectangular (top) and cylindrical (bottom) pillars with the aspect ratios, rs, used in the experiment by Fürstner *et al.*[40] The experimental WZ (CB) states are drawn as filled (open) symbols.

Fürstner *et al.*[40] reported whether the droplet on an array of rectangular or cylindrical pillars is in the WZ or CB state by changing the spacing between the pillars and the height of the pillar. To compare with their experiment, the radius of the water droplet, R (1.39 mm) from the volume of the droplet reported in their experiment[40] was set using the relation between the volume and radius of a water droplet on a surface (note that the droplet is a truncated sphere that forms a finite contact angle with the surface).[41] The calculated pressure P was 103.4 Pa. The intrinsic contact angle (120.6°) reported by Fürstner *et al.*[40] was also used.

The top of Figure 5 presents the theoretical S_Ts as lines for the arrays of rectangular pillars with three different aspect ratios (0.52, 1.03, and 1.98) used in the experiment. Note, for the S values above (below) these lines, the theory

predicts that the droplet should exist in the WZ (CB) state. Drawn as square symbols are the experimental combinations of S and H. The WZ (CB) state is drawn as a filled (empty) square. The experimental observations as to whether the droplet is in the WZ or CB state were in good agreement with theory; the experimental state for $r = 0.52$ and $H = 1$ μm is a WZ state (drawn as a black filled square), as the theory predicts. The other two data points, $H = 2$ μm at $r = 1.03$ and $H = 4$ μm at $r = 1.98$, were found experimentally to be in the CB states, and are drawn as red and blue empty squares, respectively. These are also consistent with the proposed theory as they are below the theoretical curves drawn as red broken and blue dotted lines.

The bottom of Figure 5 shows the experimental states for the arrays of cylindrical pillars. For three different aspect ratios ($r = 1.21$, 2.24, and 4.40, drawn in different colors), the WZ or CB state of the droplet was determined experimentally for five different S values. The WZ and CB states determined in the experiment are drawn as filled and open circles, respectively. The theoretical S_Ts values are also drawn as lines. Again, for the S values above (below) these lines, the theory predicts that the droplet should exist in the WZ (CB) state. For $r = 1.21$, the experimental droplet was in the WZ state (represented as filled black circles) for all five S values considered. This is consistent with the proposed theory because these points are above the theoretical curve (black solid line). For aspect ratios of 2.24 and 4.40, the experimental droplets existed in the WZ (filled circles) or CB (open circles) states depending on S. For both aspect ratios, one of the experimental data points corresponding to the CB state was above the theoretical line. With the exception of this, the remaining data points agreed with the proposed theory. Overall, the proposed theory shows good agreement with the experiment.

Conclusion

In various disciplines, superhydrophobic surfaces decorated with micro- and nano-pillars have been used extensively. The hydrophobicity of such a pillared surface depends critically on whether the water droplet on the surface is in the CB or WZ state. Therefore, it is important to understand how the CB or WZ state of the droplet depends on the width, height, and shape of a pillar, as well as the spacing between pillars. As controlling and scanning these geometric parameters are experimentally challenging, a theoretical investigation of these pillar geometries is needed. Here, this study investigated theoretically how the surface geometry, especially the interpillar spacing, affects the WZ-to-CB transition of a water droplet for an array of rectangular, cylindrical, or ellipsoidal pillars. The threshold interpillar spacing below which the WZ to CB transition occurs was examined by varying the size and shape of the pillar. The threshold spacing for an array of rectangular pillars behaved qualitatively differently from that of an array of cylindrical or ellipsoidal pillars. The present theory was found to be in accordance with the experiments reported by Zhu *et al.*[39] and Fürstner *et al.*[40]

Acknowledgments. This study was supported by the National Research Foundation of Korea (NRF) grant funded by the Korea government (NRF-2015R1A2A2A01004208 and NRF-2014R1A4A1001690).

References

1. A. R. Parker, C. R. Lawrence, *Nature* **2001**, *414*, 33.
2. W. Duan, A. Xie, Y. Shen, X. Wang, F. Wang, Y. Zhang, J. Li, *Ind. Eng. Chem. Res.* **2011**, *50*, 4441.
3. B. Shin, K.-R. Lee, M.-W. Moon, H.-Y. Kim, *Soft Matter* **2012**, *8*, 1817.
4. K.-C. Park, H. J. Choi, C.-H. Chang, R. E. Cohen, G. H. McKinley, G. Barbastathis, *ACS Nano* **2012**, *6*, 3789.
5. R. Blossey, *Nat. Mater.* **2003**, *2*, 301.
6. A. Solga, Z. Cerman, B. F. Striffler, M. Spaeth, W. Barthlott, *Bioinspir. Biomim.* **2007**, *2*, S126.
7. A. Marmur, *Langmuir* **2004**, *20*, 3517.
8. W. Barthlott, C. Neinhuis, *Planta* **1997**, *202*, 1.
9. L. Feng, S. Li, Y. Li, H. Li, L. Zhang, J. Zhai, Y. Song, B. Liu, L. Jiang, D. Zhu, *Adv. Mater.* **2002**, *14*, 1857.
10. Y. M. Park, M. Gang, Y. H. Seo, B. H. Kim, *Thin Solid Films* **2011**, *520*, 362.
11. N. J. Shirtcliffe, G. McHale, S. Atherton, M. I. Newton, *Adv. Colloid Interface* **2010**, *161*, 124.
12. D.-H. Kim, Y. Kim, J.-W. Kang, S. W. Hong, D. Lee, C.-R. Cho, S.-H. Kim, D.-W. Lee, J.-M. Kim, *J. Micromech. Microeng.* **2011**, *21*, 075024.
13. M. Nosonovsky, B. Bhushan, *Microelectron. Eng.* **2007**, *84*, 382.
14. D. Öner, T. J. McCarthy, *Langmuir* **2000**, *16*, 7777.
15. S. M. Kang, S. M. Kim, H. N. Kim, M. K. Kwak, D. H. Tahk, K. Y. Suh, *Soft Matter* **2012**, *8*, 8563.
16. A. Tuteja, W. Choi, J. M. Mabry, G. H. McKinley, R. E. Cohen, *Proc. Natl. Acad. Sci. U.S.A.* **2008**, *105*, 18200.
17. N. A. Patankar, *Langmuir* **2003**, *19*, 1249.
18. R. N. Wenzel, *Ind. Eng. Chem.* **1936**, *28*, 988.
19. A. B. D. Cassie, S. Baxter, *Trans. Faraday Soc.* **1944**, *40*, 546.
20. D. Quéré, A. Lafuma, J. Bico, *Nanotechnology* **2003**, *14*, 1109.
21. B. Bhushan, Y. C. Jung, *Ultramicroscopy* **2007**, *107*, 1033.
22. Y. Kaufman, S.-Y. Chen, H. Mishra, A. M. Schrader, D. W. Lee, S. Das, S. H. Donaldson, J. N. Israelachvili, *J. Phys. Chem. C* **2017**, *121*, 5642.
23. A. Marmur, *Langmuir* **2008**, *24*, 7573.
24. N. A. Patankar, *Langmuir* **2004**, *20*, 7097.
25. D.-H. Kim, Y. Kim, B. M. Kim, J. S. Ko, C.-R. Cho, J.-M. Kim, *J. Micromech. Microeng.* **2011**, *21*, 045003.
26. N. Choudhury, B. M. Pettitt, *J. Am. Chem. Soc.* **2005**, *127*, 3556.
27. H. K. Christenson, P. M. Claesson, *Science* **1988**, *239*, 390.
28. X. Huang, C. J. Margulis, B. J. Berne, *Proc. Natl. Acad. Sci. U.S.A.* **2003**, *100*, 11953.
29. G. Hummer, J. C. Rasaiah, J. P. Noworyta, *Nature* **2001**, *414*, 188.

30. K. Leung, A. Luzar, *J. Chem. Phys.* **2000**, *113*, 5845.
31. K. Lum, A. Luzar, *Phys. Rev. E* **1997**, *56*, R6283.
32. S. Singh, J. Houston, F. van Swol, C. J. Brinker, *Nature* **2006**, *442*, 526.
33. H. Kim, J. K. Saha, J. Jang, *J. Phys. Chem. C* **2012**, *116*, 19233.
34. H. Kim, S. I. Lee, M. A. Matin, Z. Zhang, J. Jang, M. Y. Ha, J. Jang, *J. Phys. Chem. C* **2014**, *118*, 26070.
35. H. Kim, M. A. Matin, J. Jang, Z. Zhang, J. Jang, *Bull. Korean Chem. Soc.* **2015**, *36*, 447.
36. Z. Zhang, H. Kim, M. Y. Ha, J. Jang, *Phys. Chem. Chem. Phys.* **2014**, *16*, 5613.
37. Z. Zhang, M. A. Matin, M. Y. Ha, J. Jang, *Langmuir* **2016**, *32*, 9658.
38. G. Erpul, L. D. Norton, D. Gabriels, *Catena* **2002**, *47*, 227.
39. L. Zhu, Y. Feng, X. Ye, Z. Zhou, *Sensor. Actuators, A* **2006**, *130–131*, 595.
40. R. Fürstner, W. Barthlott, C. Neinhuis, P. Walzel, *Langmuir* **2005**, *21*, 956.
41. R. Tadmor, *Langmuir* **2004**, *20*, 7659.

